Beaming of Energy via Laser for Lunar Exploration (BELLE)

Beaming Laser Power to a Rover in a Crater

Advisor
Prof. Mool C. Gupta
Langley Distinguished Professor & Director for NSF I/UCRC Laser Center

External Advisor
Dr. Paul Jaffe
Electronics Engineer, Spacecraft Engineering Department/Space Electronics Systems Development, U.S. Naval Research Laboratory

Team Members

Jacob St. Martin (4th year)
Mechanical Engineering
Team Leader & Design

Julia Rudy (3rd year)
Computer Engineering
Rover & Gimbal Tracking

Rex Serpe (3rd year)
Computer Engineering
Laser Tracking

Keerthi Radhakrishnan
Computer Engineering
Charge Controller

George Wilkes (Ph.D.)
Electrical Engineering
Laser, Optics, & Photovoltaics

Edward Lee (2nd year)
Electrical Engineering
Data Representation

David Chen (2nd year)
Electrical Engineering
Thermal & Radiation

November 29, 2020

Team Members

Prof. Mool C. Gupta

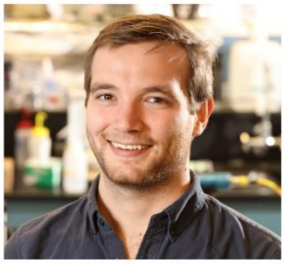
George Wilkes

Jacob St. Martin

Rex Serpe

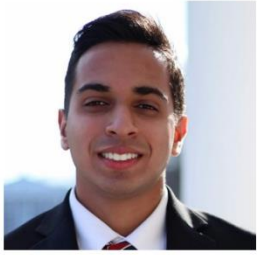
Keerthi Radhakrishnan

Julia Rudy

David Chen

Edward Lee

Dr. Paul Jaffe

Table of Contents

Abstract

1. Introduction

1.1. Problem Statement

1.2. State of the Art

1.3. Summary of the Project (Quad Chart)

2. Project Description

2.1. Design Considerations and Assumptions

2.1.1. PSR

2.1.2. Moon Dust

2.1.3. Thermal Management

2.2. Mass, Size, and Power Specifications

3. Laser Power Beaming

3.1. Laser and Optics

3.2. Photovoltaics

3.3. Tracking Circuitry

3.4. Charging Circuitry

4. Laser Beam Tracking
4.1. Retroreflection
4.2. Software
4.3. Gimbal System
4.3.1. Gimbal Design
4.3.2. Gimbal Tracking
5. Testing and Results
5.1. Proof of Concept Testing on Earth
5.2. Challenges
5.3. Testing Environment
5.4. Timeline
5.5. Budget
5.6. Safety Plan & Protocols
6. Path to Flight
6.1. Overview
6.2. Hardware Design
6.3. Optics
6.4. Software
6.5. Photovoltaic Cell Performance Optimization
6.6. Radiation Control
6.7. Thermal Control

7. **Conclusions**
8. References

Abstract

In order to address the future power generation needs for scientific exploration of the lunar permanently shadowed regions, a novel laser power beaming approach is demonstrated. An undergraduate multidisciplinary student team with expertise in electrical engineering, mechanical engineering, computer science, and optics was assembled to address the NASA power beaming challenge. Power can be beamed from the continually sunlight illuminated rim of the crater using a high-efficiency, high-power laser to a distant asset in the permanently shadowed crater interior, where water ice is expected to be plentiful. Expansion and collimation optics were used to reduce laser beam divergence at these long distances of ten kilometers. Beam scanning systems, as well as retroreflectors on the asset, are used to locate and track a mobile asset with a quadrant arrangement of photodetectors. A gimbal-mounted photovoltaic receiver was tracked through the illumination source and converted the optical power to electrical power for use by the asset's battery system and other scientific instruments. A custom printed circuit board tracked the maximum power point of the photovoltaic array and provided the power for charging of the asset's battery. Full-scale integration of all components was demonstrated through the powering of a moving rover. The project examined the design considerations, measurement of component-level performance, evaluation of integrated system performance, and future opportunities to further improve the system. In addition, a publication is being prepared for a refereed optics journal detailing our system and findings.

1. Introduction

1.1 Problem Statement

Lunar polar craters, such as Shackleton at the south pole, have rims that are illuminated for over 200 Earth days due to the 5° ecliptic tilt of the moon about its orbit. However, the 4.2 km deep crater interior lies in perpetual darkness due to the low incident angle of the Sun. These regions, called the permanently shadowed regions (PSRs), remain at average temperatures of 100 K due to the Moon's lack of atmosphere and lack of sunlight insolation in these regions. Water ice and other volatiles are believed to be trapped in these regions [1] due to the low temperatures, indicating that the frozen water has existed for potentially billions of years untouched by solar radiation. NASA and other space agencies have shown increased interest in the investigation of this ancient lunar ice located in the 3.6 billion-year-old crater, as it can provide a window into our early solar system, which itself is only 4.6 billion years old.

However, exploration of the PSRs is particularly difficult given the harsh PSR environment. Extremely low temperatures (<100 K), the lack of solar illumination, and the large crater diameter (~20 km) of these regions limit the ability of instruments to explore this region and the type of power systems that are available to support them. The general-purpose heat source radioisotope thermoelectric generator (GPHS-RTG), which has been used in the Cassini-Huygens, New Horizons, Galileo, and Ulysses missions [2], are reliable for larger platforms, but they have a low specific power, low efficiency, large mass, high cost, and long lead times for implementation. Additionally, small vehicles rely on batteries or other chemical storage, limiting their operational lifetime and the range they can travel without recharging. Tethers to the asset are heavy, voluminous, complex to deploy, and suffer from large voltage drops with distance—problems which are exacerbated by the >10 km distance from the crater rim, where sunlight is plentiful for photovoltaic power generation, to the crater bottom in the PSR, where the power is needed.

Therefore, wireless power transmission is of particular interest for PSR missions because it can avoid the shortcomings of the technologies listed above while also maintaining

reconfigurability and adaptability for changing mission and power requirements. A single beam source could power multiple, distant targets when coupled with a steering and targeting system. This beam source can be powered by photovoltaic panels at the perpetually illuminated rim of the crater and then continually transmitted to a receiver on an asset within the PSR. This energy could be used continuously or to charge batteries when needed. In this regard, both microwave frequency and laser transmitters have been previously considered for power beaming, where the former is less susceptible to atmospheric attenuation, and the latter can utilize smaller transmitters and receivers [3][2]. Therefore, due to the lack of atmosphere on the moon, the need for reduced weight on the asset, and the large, multi-kilometer distances at which the power must be transmitted—laser power beaming is the ideal technology.

This technical report demonstrates a laser power beaming method and identifies key strategies to increase the overall system efficiency that remain within design constraints for potential lunar missions. It also describes a beam steering system that can track moving objects such as rovers in the PSR using retroreflectors and a quadrant detector. The overall system includes a high-power laser, beam steering and tracking, photovoltaic receiver, receiver illuminance tracking, battery charging systems, and design considerations for each system for future lunar missions. These systems can be scaled and adapted to increase the laser transmitted power, the receiver size, and the power requirements of the asset.

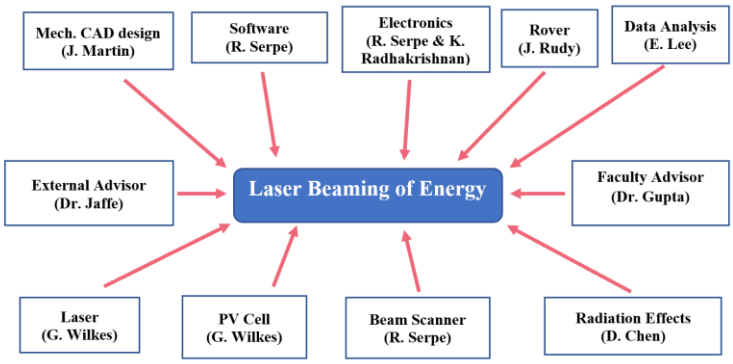

Figure 1. Multidisciplinary team member contributions.

1.2 State of the Art

Current terrestrial demonstrations of the laser beaming concept are still in the early technology readiness level (TRL) stages. During the last three decades, the average power of diode lasers has increased exponentially, while their average price has decreased exponentially. Diode lasers have reached efficiencies of 73% in the lab and >55% commercially, with laser wavelengths of 920-980 nm having the highest efficiency due to their low differential series resistance and high thermal conductivities [4]. Because of these factors, less input power is lost thermally, reducing the thermal conditioning requirements of these systems, which is important in energy-starved environments that also have a lack of atmosphere for convective cooling.

Multijunction-photovoltaic receivers have reached efficiencies >40%, with significantly increased current outputs when concentrated light, such as laser beams, illuminates them. This is typically described as the spectral response in terms of the photovoltaic output current versus the input laser power wattage (A/W). This spectral response has a peak with input wavelengths that are near but just above the energy bandgap energy of the cell, which is in the 900–1100 nm region for silicon and InGaAs receivers. Additionally, by using energy just above the bandgap, less of the excess energy is lost thermally, allowing for higher conversion efficiencies and less heating of the cells themselves, which have significant losses in voltage with increased temperature.

When the laser is coupled with beam control optics and collimating lenses, it can be beamed for long, kilometer distances with minimal divergence. Beam director systems have achieved point accuracies in the microradian range, which are necessary for locating distant targets in a lunar crater accurately. Using the current state of the art technologies, it is currently estimated that the end-to-end efficiency, including losses of the laser and photovoltaic, of this beaming system would be in the 3–5% range; however, this has yet to be demonstrated terrestrially. This efficiency could be further improved through additional R&D.

Both powers beaming and optical tracking have significant applications in the energy and aerospace industries, including the transmission of power both to and from the ground, spacecraft, aerial vehicles, satellites, rovers, and other exploratory equipment. Wireless power transmission could also play a vital role in providing power to remote locations or in the event of natural disasters when traditional power systems are destroyed. Laser power beaming to a photovoltaic receiver has been previously demonstrated by PowerLight Technologies and Prof. John Federici's group at the New Jersey Institute of Technology. These demonstrations include successfully beaming 400 W of power over 1 km [5], powering a quadcopter UAV for over 12 hours, and powering a small remote-controlled vehicle [6]. Laser object tracking and ranging using retroreflectors and beam scanners is a commercially proven metrology technology. Additionally, Mirrorcle Technologies has a commercially available MEMS mirror scanner that can track retro-reflective targets exceptionally well, but MEMS systems are currently unable to handle continuous, high laser power with large beam diameters. The key novelty in our BELLE's approach is the integration of all of the components while focusing on power beaming applications in lunar PSRs. Assessing power, range, and accuracy limitations of the beaming system are demonstrated. Most of these concepts have been demonstrated individually and through integration, so the risk for adoption by NASA is relatively low.

Additionally, the goal of this system is to have each of the components deploy autonomously without the need for human input or control. Utilization of tracking elements at both the beam source and the receiver, the power can be beamed successfully without communication between the laser source and the rover. This enables the versatility of the system with the opportunity to add additional laser sources or mobile assets at later dates without having to update the previous systems. The advantage of this work is that it is directly applicable to the lunar PSR environment for direct implementation by NASA, given further validation and TRL improvement.

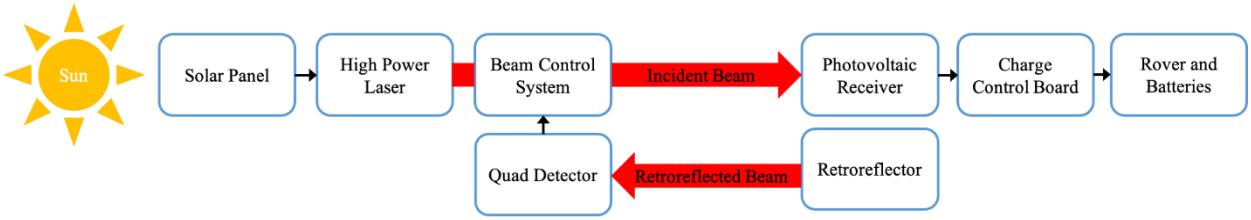

Figure 2: Flow Chart of BELLE System

Beaming of Energy via Lasers for Lunar Exploration (BELLE) is a system designed to solve the issue of powering equipment for exploration and operation in lunar permanently shadowed regions (PSRs). Traditionally, exploratory equipment would either directly use solar energy or would utilize nuclear energy. Due to a lack of sunlight, solar energy cannot be used, and nuclear energy is both expensive and unstable. Also, direct sunlight could not be transmitted at multi-kilometer distances due to the large divergence of the sunlight beam. BELLE solves this energy problem by utilizing solar energy in an illuminated area along the rim of a crater and

beaming the energy to equipment with a high-powered laser. The energy is then recollected and converted back into electrical energy where it can be used. BELLE uses an optical retroreflective tracking system to locate and follow any equipment.

BELLE could revolutionize lunar exploration and has an impact that extends even beyond the moon. The lunar PSRs are regions of the moon that never receive sunlight; these areas are significant because they contain ice that is believed to have been deposited by comets and retained by the extremely low temperatures of the PSRs. This ice is so important because it can be used to support lunar habitation or for electrolysis into liquid oxygen fuel. This habitation and refueling capability is a key component to deeper space exploration.

There are many components that must be integrated to create a working tracking system. While developing BELLE, the primary systems being investigated were laser power beaming and optical tracking.

1.3 Summary of the Project (Quad Chart)

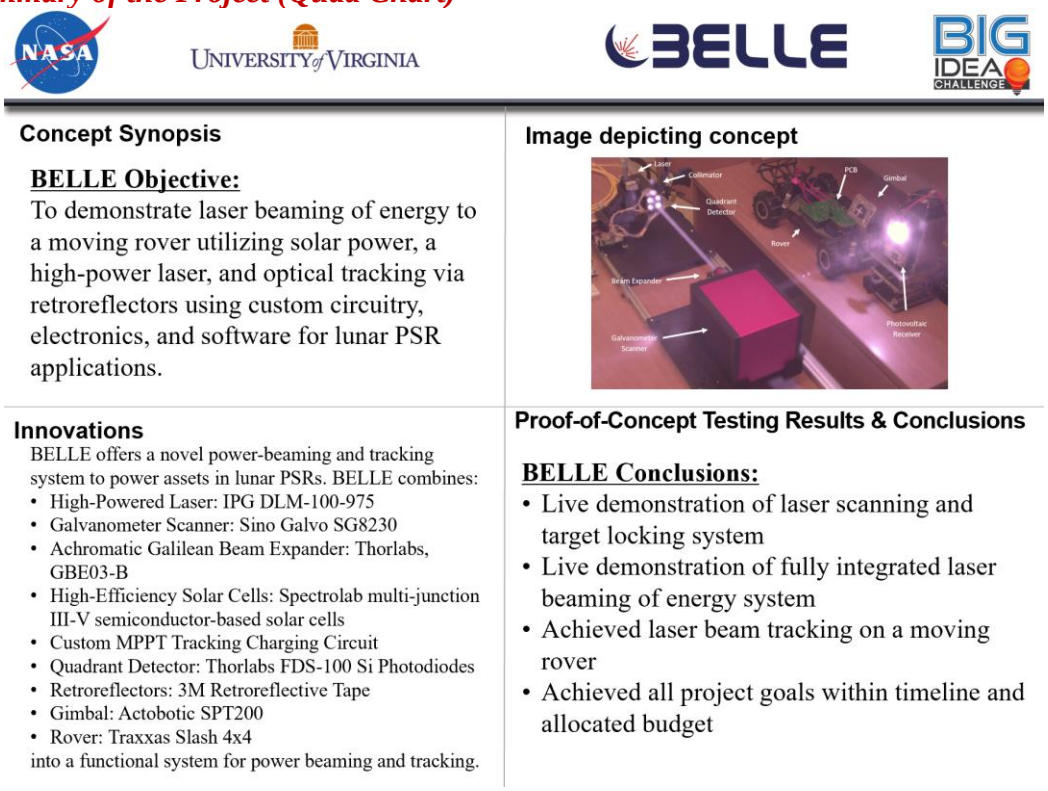

2. Project Description

2.1 Design Considerations and Assumptions

2.1.1 PSR

The BELLE system can be deployed directly on top of a lander located at the crater rim as there are no moving parts except for the rover and the motorized mirrors inside of the galvanometer scanner system. The beaming system itself is relatively compact and can fit within a 95 x 30 x 16 cm volume. The rover could travel in this same lander and subsequently drive into the PSR or deploy separately and land in the PSR. Additionally, the BELLE system could be robotically placed on top of a tall tower on the edge of the crater to increase laser "visibility" into the PSR. Potentially integration with the MELLTT tower developed by the team at MIT would enable a

compact method of doing this. Ideally, the BELLE system would be located at a rim position, which provides an ideal view of the entire crater. For the Shackleton crater, the diameter is 21 km with a depth of 4.2 km [7]. The interior terrain was imaged by the Japanese SELENE spacecraft and consisted of a 30° slope that leads down to a 6.6 km diameter floor [7]. The floor is a slightly raised mound with a 200 m central peak. While there is potential for the rover to enter a region that is not visible from the rim due to the roughness of the terrain, the majority of the crater should be visible from the rim.

2.1.2 Moon Dust

BELLE is an enclosed system, which prevents dust accumulation. Furthermore, other precautions such as a PLZT driven dust mitigation techniques could be put in place to keep optics clean.

2.1.3 Thermal Management

Heating issues caused by the high-power fiber laser in proof-of-concept testing on earth would be less problematic on the moon due to the lunar surface's extremely cold ambient temperatures. However, since temperatures at the rim of Shackleton can reach 100 °C during the day, the laser system should be encased in a reflective enclosure to reduce heating.

2.2 Mass Size and Power

Table 1. Component Dimensions, Mass, Power and Total Volume, Weight, and Power.

Components	Length (cm)	Width /Radius (cm)	Height /π • R (cm)	Mass (g)	Power Max (W)	Number	Total Volume (m^3)	Total Weight (kg)	Total Power (W)
PV Cell for Sun	7.72	7.72	0.03	5.01	+2.42	150	0.23	0.75	+363.0
Laser System	27.00	25.50	7.50	6000.0	-235.0	1	5.16	6.00	-235.0
Beam Expander	8.55	2.25	7.07	130.0	N/A	1	0.14	0.13	N/A
Galvo Scanner	21.50	18.300	15.80	7650.00	-96.0	1	6.22	7.65	-96.0
Microcontroller	13.30	7.00	1.00	117.4	-1.5	2	0.19	0.23	-3.0
Receiver Cell	2.2	2.0	0.5	10.0	+10	1	< 0.01	0.01	+10.0
Charge Board	15.5	13.2	0.236	54.1	-0.5	1	0.05	0.05	-0.5
Rover	56.7	29.6	21.3	2159	-6.6	1	35.75	2.2	-6.6
Gimbal	5.08	10.16	12.9	948	-0.7	1	0.67	0.95	-0.7
Photodiodes	3.20	1.40	1.00	2.8	-1.5	4	0.02	< 0.01	-6.0
						Total	11.98	14.83	+25.2

3. Laser Power Beaming

The integrated system consists of several components such as a high-power laser, photovoltaic cell, laser beam scanning system, rover, and quad detector for beam locking, and required the development of electronic circuits and software. In the following section we describe the functionality and characteristics of each component.

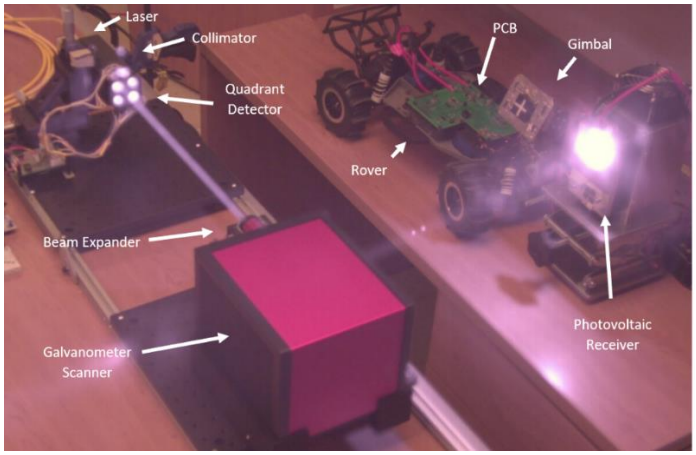

Figure 3. BELLE system design

3.1 Laser and Optics

The primary component of our system will be a laser source located at the rim of the crater. This laser utilizes power generated at the rim of the crater, ideally via photovoltaic power generation. This is feasible considering the rim receives over 200 Earth days of illumination due to the 5° ecliptic tilt of the moon about its orbit. This electrical power is then converted to optical power with the laser and beamed to a distal target in the lunar PSR, where sunlight is absent.

There are a variety of factors to consider when selecting an appropriate laser for power beaming. The categories of lasers that could be considered for this task include semiconductor diode lasers and fiber lasers, both of which can produce kilowatts of laser power. Overall, diode lasers are capable of higher electrical-to-optical efficiencies than fiber lasers but have significantly greater beam parameter products (BPP), causing increased beam divergence at large distances. This is because fiber lasers commonly require a pump diode laser for the fiber, so their efficiency is a result of a two-stage process (electrical-to-optical and optical-to-optical). Diode lasers typically have poor BPP as they rely on a series of diode bars coupled into multimode fibers. High power fiber lasers, like common Nd:YAG lasers, are typically single-mode and have far better BPPs. Without cooling, diode lasers typically have a lower overall weight, but cooling systems are far more complex than fiber lasers since the output can be severely affected by temperature. However, due to the unique cooling requirements at the lunar south pole and *in vacuo*, further consideration is needed on the cooling systems for each laser source.

Of diode lasers available, those in the 920–980 nm spectral range have the highest power conversion efficiencies (up to 73%) due to low differential series resistance and high thermal conductivities [8]. Meanwhile, the photon conversion efficiency of fiber lasers is >90%, but they rely on pump diodes, which have equivalent conversion efficiencies of standard diode lasers. In high-power commercial units, this results in wall plug efficiencies of around 55% and 53% for diode and fiber lasers, respectively. Because of diode lasers enhanced efficiency, they are ideally suited for energy-starved applications in the lunar PSRs as well as reduced cooling requirements

for energy lost thermally in the electric-to-optical conversion process. The laser selected for this project was an IPG DLM-100-975 fiber-coupled direct diode laser with an adjustable power output up to 100 W and laser wavelength of 975 nm, as shown in Figure 4. At full power, this laser consumes 235 W while delivering 105.5 W, giving it a wall plug efficiency of 45%. It has an operating ambient temperature range of 0–50°C with a storage temperature of -40–75 °C, so thermal conditioning may be needed to keep it in its operating range with the daily thermal cycling on the moon. The unit has dimensions of 270 x 75 x 255 mm, with a mass of 6 kg. Additionally, the laser system has a red wavelength guide beam for alignment purposes and quick checking of beam location with the scanning system.

Figure 4: IPG DLM 100 975

The diode laser is coupled to a 200 µm core diameter multimode fiber. The multimode profile of the fiber helps to spread the beam intensity over a larger area and reduce high laser intensities at the Gaussian peak, normally seen in single-mode fibers (commonly used in high-efficiency fiber lasers), that could cause damage to the receiver PV module at the center of the beam. This fiber is coupled to an 8 mm input beam diameter collimator, with an approximate divergence of 10 mrad. A custom housing was 3D-printed for the collimator head so that it could be attached to a three-axis XYZ translation stage to allow for alignment with subsequent optical components. This housing also contained four recessed areas for the photodiodes used for tracking. Low divergence is hard to achieve with multimode beams, especially at higher wavelengths. Larger beam diameters help to reduce divergence because of the fast and slow axis of diode lasers, causing diffraction or divergence of light when concentrated in a small area. As a general rule, the divergence is halved every time the beam diameter is doubled. Therefore, a 3X achromatic Galilean beam expander with a Near-IR (650–1050 nm) anti-reflection coating was purchased to expand the beam to 24 mm (Thorlabs, GBE03-B) and reduce divergence. Galilean beam expanders are simpler, more compact, and lower cost than Keplerian expanders, and they prevent internal focusing, which is ill-suited for high-power laser applications. It has an adjustment ring to precisely tune the collimation and minimize the divergence so that the beam can travel large distances without a loss in power density. The output beam from the collimator has a 1” diameter and beam divergence of about 3 mrad. A custom housing for the beam expander was also 3D printed. The beam was profiled at a distance of 5 meters from the laser using a 1 cm^2 aperture (Ø1.128 cm) and a photodiode with a neutral density filter to protect the sensor. The sensor and aperture were translated using a linear stage from the edge of the center of the beam to the edge where there was no illumination. The beam full width at half-max was measured to be 41 mm, and the beam profile fit was non-

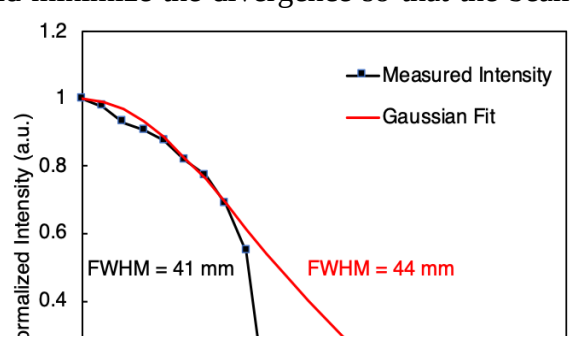

Figure 5: Measured multimode beam profile and comparison with ideal Gaussian profile.

gaussian, closer to a multimode profile as expected. The profile and its comparison to a Gaussian profile are shown in Figure 5. Additionally, the laser power was measured using a thermopile sensor (Newport, 919P-250-35) at an equivalent distance using the same 1 cm^2 aperture to measure the power density for later calculation of the photovoltaic cell efficiency. The measured power density is shown in Figure 6. Using a 41 mm FWHM beam diameter to calculate the total beam power, the measured power values match the specified values well.

The expanded beam then passed into a large area galvanometer scanner (Sino Galvo, SG8230). The scanner houses two motorized mirrors with a 980 nm reflective coating, which can translate the beam in x and y. The galvo can accommodate a 30 mm beam through its aperture and deflect the beam with mirror sizes far exceeding 30 mm. No focusing lens was used on the galvo scanner in order to keep the beam at its 24 mm size. The motorized mirrors use digital controls in the XY2-100 format. The scanner has a linearity of 99.9%, scan angle of ±15°, resolution of 12 µrad, and repeatability of 8 µrad. The accuracy of typical galvanometer scanners is limited by their pointing accuracy, typically on the order of 40-50 µrad, and mechanical repeatability, typically around 10 µrad for commercial systems. Since the Shackleton crater has a diameter of 20 km and a depth of 4.5 km, the linear distance from the rim to the bottom of the crater is just above 10 km. Using commercial scanners, it is estimated that the beam would be accurate to 400 mm at that distance, which would be quite a large PV receiver for small assets. Using the galvo system in this work, the pointing accuracy would be roughly 120 mm at this distance. The scanner has dimensions of 215 x 183 x 158 mm with a motor weight of 750 g. The scanner could be utilized without its housing to reduce weight and potentially increase the scan angle's capabilities to allow for a broader field for object tracking. An image of the scanner and the motorized mirrors is shown in Figure 7.

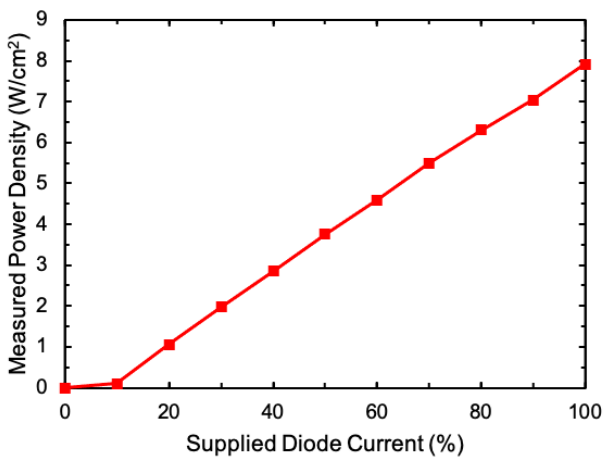

Figure 6: Measured laser power density as a function of diode current percentage using a 1 cm^2 aperture.

It took several weeks to find the ideal galvanometer scanner; nearly all commercial scanners cannot handle a 24mm diameter beam, NIR wavelength, and 100 W optical power. An ideal galvanometer scanner for the BELLE proof-of-concept would be custom-built.

Figure 7: Galvo scanner housing and servo-controlled motorized mirrors.

3.2 Photovoltaics

The system architecture for our project involves the efficient collection of sunlight and converting it into electric power. The generated electric power operates a high-power laser, which can be beamed into the crater. A solar module mounted on the rover collects the laser light and converts it back into electric power for its operation.

Photovoltaic cells are used for sunlight to electricity conversion and also for the conversion of laser light to electric power. For efficient conversion of laser light to electric power, the solar cell semiconductor material should have a bandgap close to the laser wavelength. Based on the availability of high-power lasers and high-efficiency solar cells, a laser wavelength of 975 nm was selected. We investigated multijunction silicon solar cells and III-V photovoltaic cells. The vertical multi-junction silicon solar cells have an efficiency of around 35% at the laser wavelength. The multi-junction III-V semiconductor-based solar cells also have an efficiency of 35% and can work better at concentrated light, such as light from the laser source. This is aided by their direct bandgap allowing for more efficient absorption and collection while preventing increased temperatures at high light concentrations. After some investigation, Dimitri Krut at Spectrolab Inc. in California agreed to provide some 1.1 cm x 1 cm solar cells at no cost to the project. Spectrolab is one of the major companies which supports NASA's space solar cell needs [9]. The provided cells are 2-junction metamorphic concentrator solar cells consisting of GaInAs on a Ge substrate with a top cell bandgap around 1.1 eV. A single cell was mounted on a copper substrate using silver conductive paste (Structure Probe Incorporated) for initial illuminated current-voltage testing, as shown in Figure 8 (a). The spectral response of the cell was provided to us by Spectrolab, as shown in Figure 9 (b), and shows that at our illumination wavelength (975 nm), it should be approximately 0.68 A/W. The laser power was beamed at the cell, and probes were placed on the anode and the copper block, which was in electrical contact with the cathode via the silver paste, as shown in Figure 9 (c). Figure 9 (d) shows the dark, Class A Xenon lamp-illuminated and 975 nm laser-illuminated current-voltage curves. Both the laser and lamp were set to a power density of 100 mW/cm^2 to compare the performance of one sun illumination and laser illumination. The measured spectral response of 0.68 A/W matches precisely with the measured value at Spectrolab. To assess the effect of higher light intensity on cell performance, the laser power was increased, and similar I–V measurements were made. The results are shown in Figure 8 (a). Unfortunately, the Keithley 2400 system used to make the measurements had a current limit of 1.05 A, so laser powers above 1.56 W generated too much current for accurate I–V measurement, as can be seen in the truncated curve of the 1.56 W measurement. To address this and to measure the cell output at higher laser powers, a Ø2.5 mm diameter aperture was placed in front of the cell, and the current density was

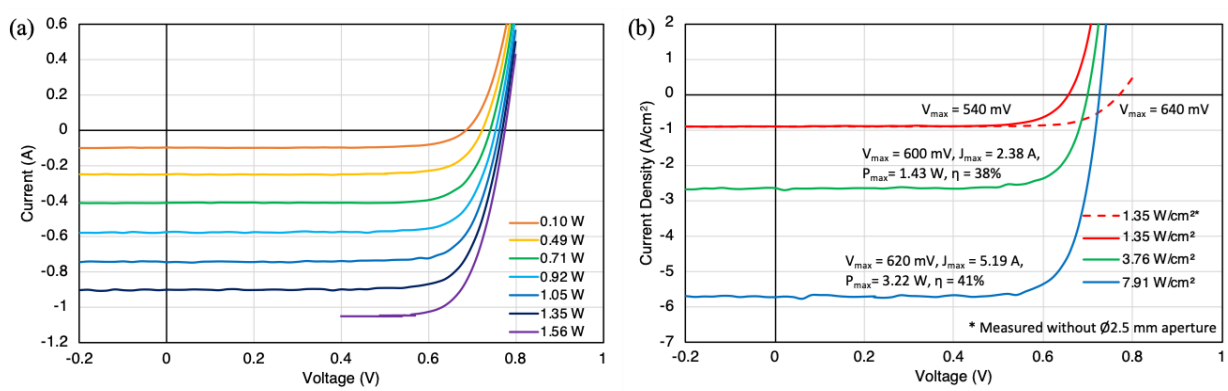

Figure 8: Current- voltage curves of (a) the full area illuminated cell at low laser powers and (b) higher laser powers.

measured assuming Ø2.5 mm of cell illumination instead of the 1.1 x 1 cm cell area. These results are shown in Figure 8 (b). One measurement was made at an identical power (1.35 W/cm^2) to the cell when it was fully illuminated to account for any differences coming from illumination through the aperture. While the current density remains constant, there is a loss on the open-circuit voltage likely due to un-illuminated areas of the cell. Still, a 40.7% efficiency was obtained at the full 105 W power laser illumination, which was interpreted as a 7.91 W/cm^2 power density through the aperture.

Because the single-cell voltage at maximum power point (V_{max}) was around 640 mV, four cells were connected in series to increase the array voltage to around 2.5 V. Since this arrangement

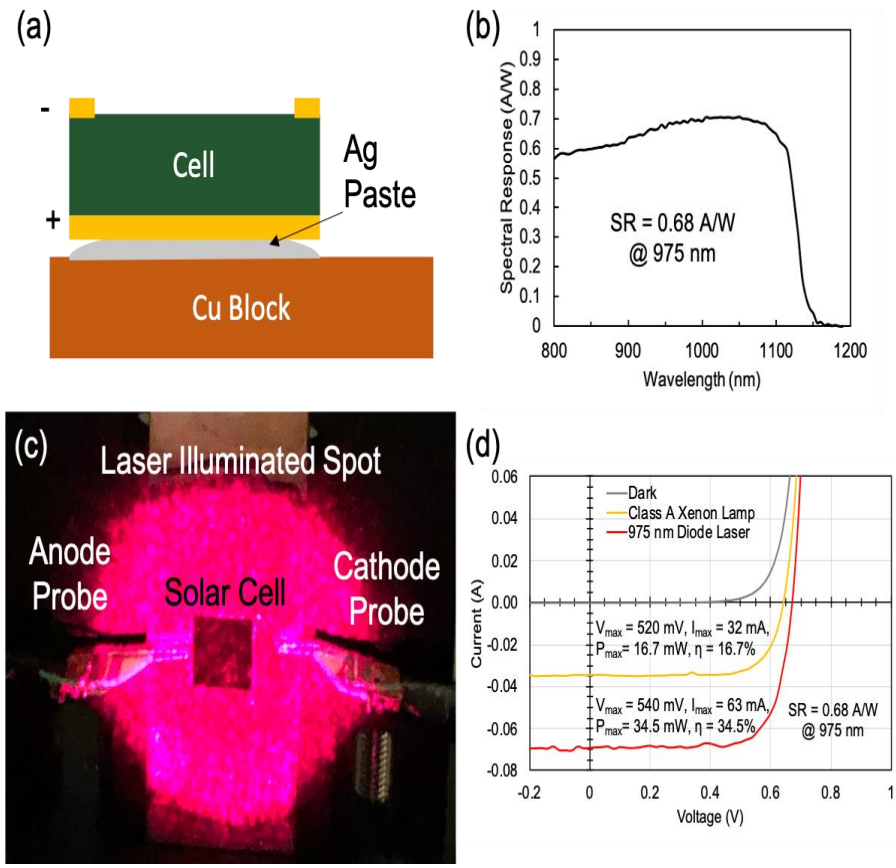

Figure 9: (a) Device structure mounted on copper block, (b) spectral response of solar cell from Spectrolab, (c) image of laser illuminated cell with probes for testing and (d) dark and 100 mW/cm^2 - illuminated current-voltage curves of the cell.

could not be mounted on a copper block without shorting the cells at their cathodes, a ceramic Al_2O_3 substrate was used to mount the cells. Silver foils (100 µm thickness) were laser cut into pads and wires to interconnect the cells in series while maintaining the smallest distance between cells as practicable. It was necessary to keep the cells close together because of the relatively tight laser spot. Mounting of this arrangement consisted of applying the silver paste to the ceramic substrate and then placing the first silver strip down for the cathode of the first cell in series. The silver paste was used on top of this pad, and the first cell was placed on top of this and cured at 120 °C for 10 minutes. Next, the anode strip was applied to the first cell using silver paste under the fingers of the subsequent pad. This was done sequentially with curing steps in between.

Additional cells can be connected in series or parallel to obtain the desired voltage and current required for the operation of the asset. A high-gauge wire is then soldered to the exposed silver strips and connected to the custom charge controlling PCB. The thinnest part of the silver interconnection was at the fingers at each anode and resulted in roughly an 8 μΩ series resistance loss at each. Because the 4-cell series arrangement was square and the beam profile was circular, there are some optical losses where the edges of the beam were simply reflected off of the substrate and not collected by the cell. When calculating the efficiency of the array, the power density and array area were used to calculate the incident power, not the entirety of the laser power. Beam shaping optics would be necessary for further evaluation.

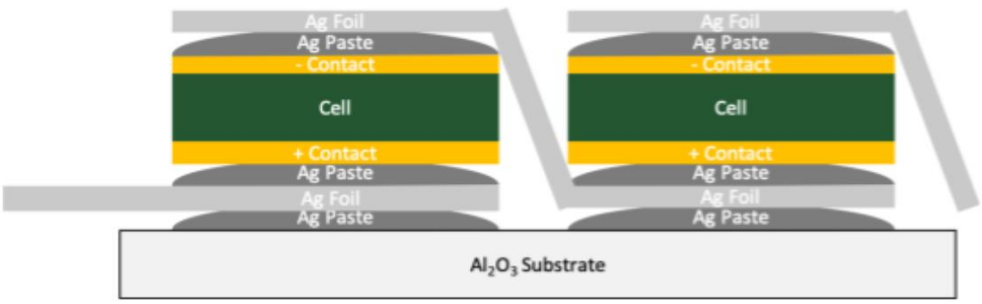

Figure 10:Cross-sectional view of array interconnection for two cells in series.

Current-voltage measurement of the series integrated cells were measured under a laser illumination of 19 W, which was the maximum laser power they could be measured at, while the I_{SC} remained under 1.05 A of current for the Keithley 2400 SMU. The results are shown in Figure 11. There is some fill factor loss when compared with the single cell, likely due to series resistance losses stemming from the interconnection of the cells. This results in a V_{MAX} of 2.452 V, J_{MAX} of 0.777 A, and efficiency of 32.62% at less than a fifth of the full laser power. While current-voltage sweeps could not be done at higher laser powers with this system, a multimeter was used to measure the V_{OC} and I_{SC} of the array at full laser power (105 W), obtaining 2.992 V and 4.95 A, respectively. Assuming an identical fill factor (0.67) from the 19 W I–V measurement, this would mean that the array can produce 9.93 W at an efficiency of 31.39% under 31.64 W of P_{IN} laser illumination.

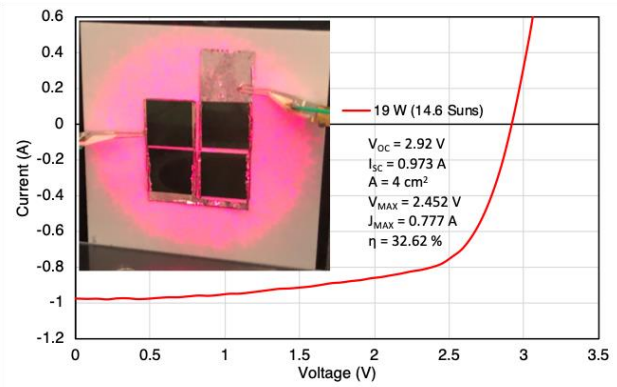

Figure 11. Current-voltage measurement of the series arrangement of four Spectrolab InGaAs/Ge cells at 19 W of laser power. The inset shows an image of the cells with illumination by the laser guide beam.

3.3 Tracking Circuitry

The performance of the system relies on the ability to detect light from retroreflectors on the rover, which is often faint and embedded in an environment with significant noise. In order to detect this signal, 4 Thorlabs FDS100 silicon photodiode cells were placed near the laser housing, as shown in Figure 12. The sample circuit from the FDS100 data sheet was used to process and filter the output of these diodes. A very large load resistance of 820kΩ was selected, which allowed even faint reflections to be amplified and detected. Additionally, a high pass filter implemented by

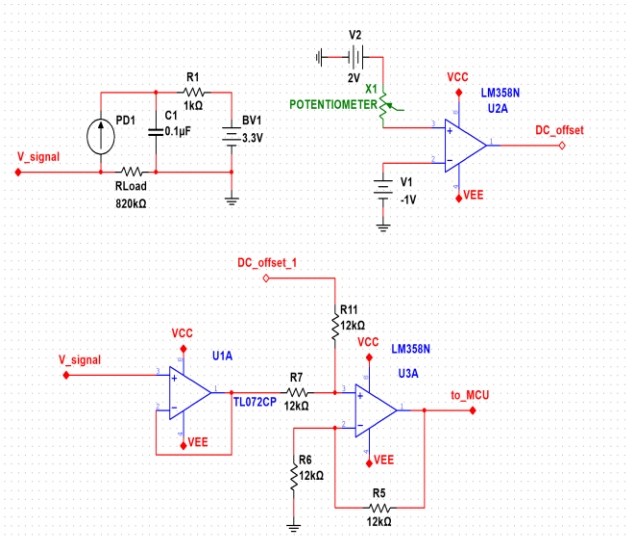

Figure 13. Photodiode processing circuitry to amplify faint signals from distant retroreflectors.

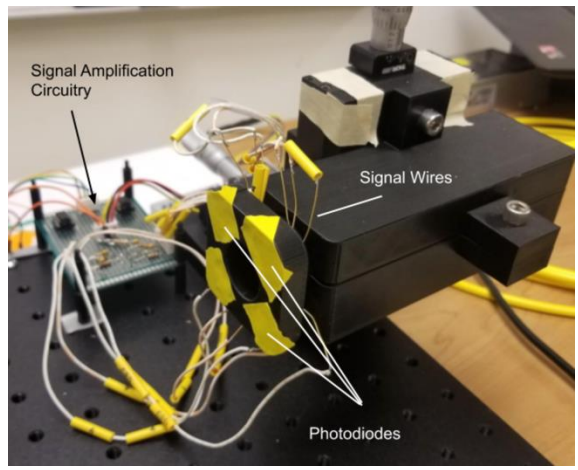

Figure 12. Photodiode sensor circuitry for detecting reflected light from retroreflectors on rover.

R1 and C1 as seen in Figure 13, was used to eliminate high-frequency noise from undesired sources such as fluorescent lights. Finally, a summing operational amplifier was implemented in order to add a DC offset to the signal reading, in case the voltage fell above or below the 0-3.3 V range of the ADC of the microcontroller. This signal was then run into an STM32 Nucleo F413ZH microcontroller, which read the sensor signals, interpreted the readings, and adjusted the tracking algorithm accordingly.

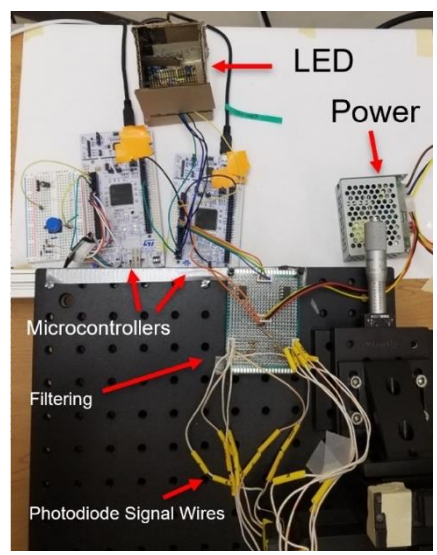

Figure 14. Full system circuitry, including two microcontrollers, the power source, filtering and amplification circuitry, and photodiodes with signal wires.

To determine the battery charging state and demonstrate it visually, a battery LED indicator circuit was designed and created. This circuit used the LiPo battery's characteristic curve to determine the voltage of the battery at specific percentages: 20%, 40%, 60%, 80%. Since the LiPo Battery was a 2-cell battery (25C), the threshold voltages shown in the chart were multiplied by a factor of 2 to determine the true battery percentage relative to the voltage. Four comparators were used at threshold voltages 6 V, 6.8 V, 7.1 V, and 7.3 V for 20%, 40%, 60%, and 80%, respectively. When the battery voltage was above the threshold value, an

LED was illuminated to indicate that the battery charging level percentage was greater than the threshold percentages.

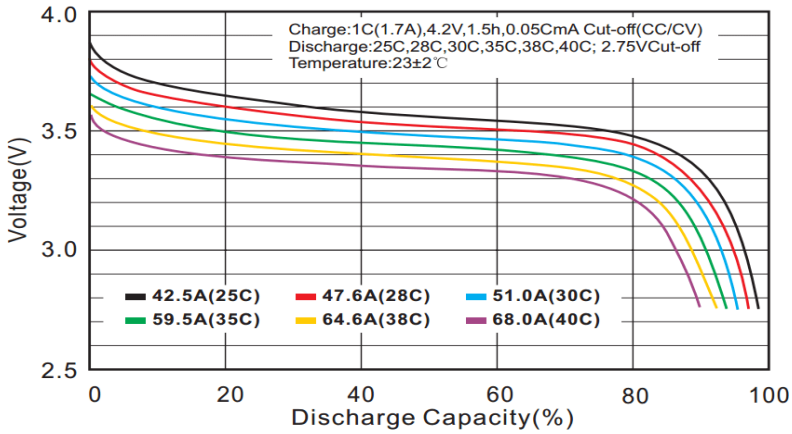

Figure 15: Characteristic battery voltage curve of LiPo Battery. [15]

To show the current battery voltage and current, a SunFounder Serial LCD Module display was used. This LCD monitor was controlled by an Arduino Nano. Since the Arduino Nano can only read voltage values up to 5 V, the voltage of the battery had to be stepped down using a voltage divider and refactored in the software implementation of the LCD to display the correct voltage. The current value displayed is the current going into the PCB from the solar cell and is calculated by measuring the voltage drop across a sense resistor and dividing it by the resistor value.

3.4 Charging Circuitry

Due to the characteristics of the solar cells used in our application, the output of the array is generally near 2.8 V and at currents of up to 4 A. This is not well suited for charging 6.8 V lithium polymer batteries, like the ones used to power our rover. Thus, a charge controller was designed to convert the high current, 2.8 V output of the array into 6-8 V, slightly lower current output using a boost converter and various integrated circuits for charging. The layout of this PCB is shown in Figure 16. The PCB also includes an integrated ATMega328-P microcontroller, which performs the gimbling operation to orient the solar array in the direction of the beam to maximize power delivery. Shown in Figure 16 is the fabricated board and the array mounted on a thermoelectric device to provide additional cooling during our tests.

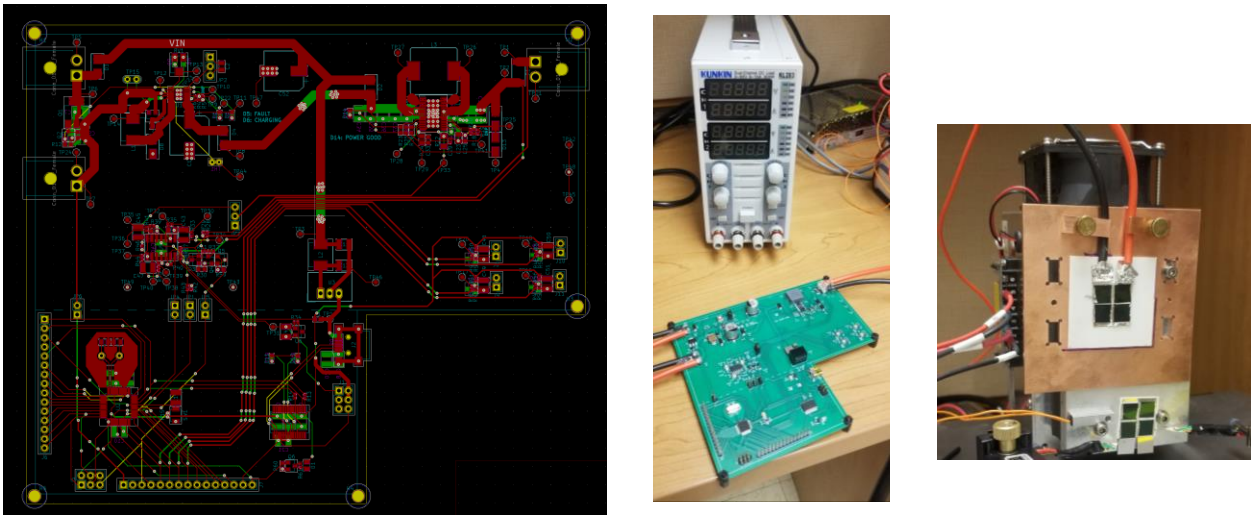

Figure 16: From left to right: PCB layout, Testing of Fabricated PCB Board, PV Array Mounted on Thermoelectric

Laser Beam Tracking

4.1 Retroreflection

In order to reflect light back from the rover to the scanning system, a high-gain retroreflective tape manufactured by 3M was placed on selected areas on the rover. Unlike a mirror, which relies on specular reflection, the retroreflectors send a beam of light back on a parallel path to the incident beam, traveling towards the detectors no matter the incident angle of the search beam. Because all other materials on the asset have a specular or diffuse reflection, only the parts tagged with retroreflective tape are tracked. This enables much higher performance tracking.

As the light travels back from the rover towards the detectors, it travels through the beam expander, opposite the direction of the original laser light. As it travels from the beam expander to the detectors, it diverges just enough to illuminate the surface of the photodiodes and provide a signal the microcontroller can detect and use to lock onto the rover.

4.2 Software

The tracking software is split between two microcontrollers, which handle the computing task in parallel to maximize system performance. This allows

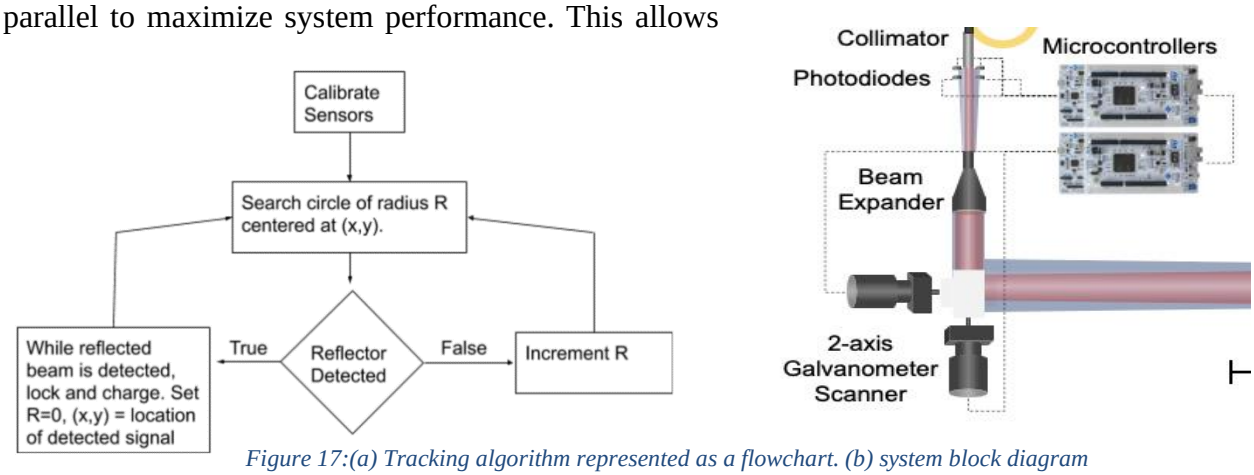

Figure 17:(a) Tracking algorithm represented as a flowchart. (b) system block diagram

one of the microcontrollers to focus the entirety of its computational power on observing the sensors and making decisions on whether a rover has been detected while not having to waste clock cycles on articulating the beam. Similarly, the scanning microcontroller can use the entirety of its processing power to search as quickly as possible without having to read from the sensors. The tracking algorithm implemented by the microcontrollers is depicted in Figure 17(a).

The scanning microcontroller (MCU) communicates with the galvanometer, spiraling out radially from the center search point. Effectively, the scanning MCU rotates in a circle of radius R, stopping very briefly at many points along the circle, while the sensor MCU reads the values of the sensors to see if a rover has been detected. If no reflected light is detected, the circle's radius is increased, and the process is repeated until a lock is found.

Once reflected light is detected by the sensors, the sensor MCU tells the scanning microcontroller to stop. The scanning MCU remains locked onto the point it was at when it was told to stop, resets the origin of the circle to that location, and brings the circle radius back to its minimum value. If the robot moves, the sensor reading drops, the sensor MCU sends a signal to the scanning MCU, which restarts the scanning process.

4.3 Gimbal System

Figure 19: 3D Printed Mount (left) and Copper Mounting Plate (right)

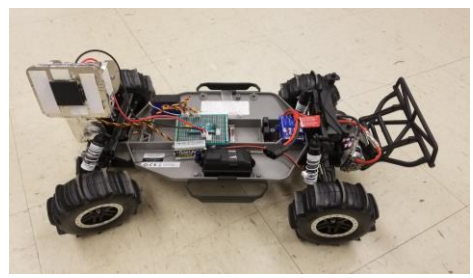

Figure 18: Gimbal Mounted on Rover

4.3.1 Gimbal Design

The gimbal used to align the PV receiver and NIR laser was a modified Actobotic SPT200, Figure 18. The gimbal went through several design iterations, including a system where the tracking was controlled by photodiodes. However, due to the high laser power, the final tracking algorithm relied only on the current and voltage readings coming from the PV receiver. Two non-continuous Hitec™ servo motors control the gimbal's yaw and pitch angles. The gimbal's current draw as it spins is summarized in Figure 20 where the average current consumption is 145 ± 60 mA. The gimbal was covered in an insulating foil to shield the 3D printed parts from the high-

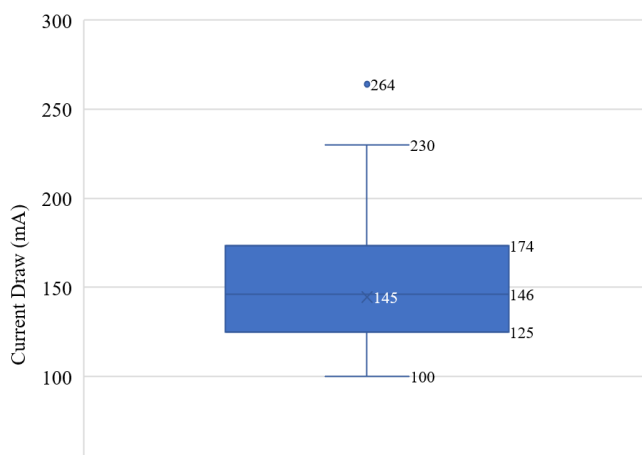

Figure 20: Consumption of gimbal during 360-degree rotation. The average current consumption is 145 mA with a 60-mA standard deviation.

powered laser, Figure 19. Two distinct mounting plates were designed: a 3D printed mount to demonstrate gimbal-tracking abilities with a silicon solar cell and a copper plate, where the PV receiver was mounted. The retroreflective tape was placed all along 360° degree of rotation around the receiver to ensure the laser would lock onto areas the gimbal could reach.

4.3.2 Gimbal Tracking

The goal of the gimbal is to center the NIR laser on the PV receiver after the beam has locked onto the rover. To achieve this goal, an ATMega328-P microcontroller continuously reads the current and voltage signals coming from the PV receiver. Until the beam is incident on the receiver, the gimbal rotates 360 degrees. Note the gimbal does not spin 360° continuously; otherwise, the wires connecting the photovoltaic cell to the PCB on the rover would tangle. As soon as the ATMega328-P microcontroller senses illumination on the cell, the gimbal stops spinning and then moves incrementally by one degree in yaw and pitch while monitoring the output from the cell. If the new position receives less illumination, the gimbal then returns to the original position and tries to move in another direction. The gimbal repeats these steps until it finds the position where the incident light is centered on the receiver. An IXOLAR™ SM730K12L silicon solar cell was used to demonstrate the gimbal tracking abilities. As seen in Figure 21, from the time the gimbal first sensed incident light on the receiver, it was able to center the beam in approximately 8-10 seconds, indicated by the steady voltage readings.

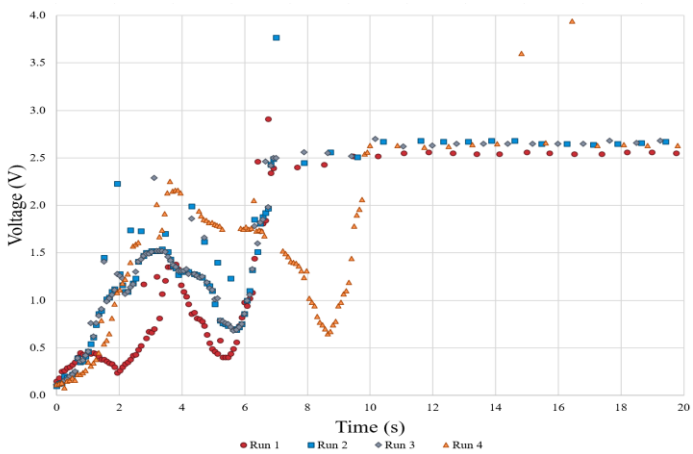

Figure 21. Voltage reading vs time of the gimbal mounted PV cell. The steady voltage shows that the gimbal is properly oriented.

4. Testing and Results

5.1 Challenges

Many challenges were faced over the course of this project, but the foremost challenge was the covid-19 pandemic. On March 11th, during spring break, the university announced that all classes would be moved online and that students were required to return home. This decision came with no notice, so we were not able to prepare for such a shutdown. Additionally, the university immediately revoked student access to all the buildings on grounds, meaning that we were unable to collect our components. Our graduate team member was unable to return to the grounds until mid-June, where they were able to begin testing of the laser and photovoltaic receiver as well as send components to the homes of the other team members.

Continuing the work from home posed new challenges, but we put forth our best effort to overcome them. The team met weekly over zoom to share progress and maintain focus. In order to continue working, the subsystems were constructed at the homes of several different team members and integrated when the team was allowed back in the labs in September. This was achieved by ordering parts to team member's houses, mailing components, and meeting regularly over zoom.

The pandemic provided significant and unexpected challenges. These challenges slowed the team down at times, but we were able to stay focused and push through the roadblocks before us, making the team stronger in the end.

Additional Challenges are summarized in the table below.

Table 2. BELLE Technical Task Schedule.

Tasks	Design Considerations and Challenges	Solution	Part #
Laser Selection	Power | Wavelength | Beam Divergence | Fiber, diode, solid state | Weight | Size | Cost | Safety | Reliability	Collimated 100 W diode laser at 975 nm wavelength expanded via a beam expander	IPG DLM-100-975. Thorlabs, GBE03
PV cell Selection	Power Conversion Efficiency | Spectral Response | Reliability | Weight | Size | Cost	High efficiency GaAs photovoltaic cell	Spectrolab multi-junction III-V semiconductor-based solar cells
Laser Beam Scanning	Resolution | Wavelength | Weight | Speed	Galvanometer scanner	Sino Galvo SG8230
Rover Selection	Weight | Ability to Mount Gimbal | Power Consumption	Remote control car	TRAXXAS 4x4 RC Car
Laser Beam Locking	Locate Object at 10 km | Receive Signal from Rover | Power Maximization	Retroreflector and photodiodes	3M Retro Reflective Tape. Thorlabs FDS100 Silicon Photodiode
Software	Galvanometer Control | Speed	Novel tracking algorithm in C++	--
Electronics	Power Conversion Efficiency | Size | Weight	Custom charging PCB	---

5.2 Testing Environment

All testing was done in Professor Gupta's lab at the University of Virginia. Ideally, it would have been better to test the system in a larger area where tracking could have been demonstrated at larger distances and over more varying terrain. However, due to the pandemic and the safety concerns associated with a high-powered class IV laser, an alternate testing location was not possible.

Due to these limitations, it was more difficult to simulate the lunar environment for testing. However, there are several ways in which BELLE would operate more efficiently in a lunar environment. For instance, due to the high laser power, the photovoltaic cells tend to heat up, and a drop in efficiency occurs despite the use of a heat sink. In a lunar environment, it would be easier to dissipate heat due to the extremely cold ambient temperatures. Additionally, the relative uniformity of the lunar regolith compared to a lab space would increase the accuracy of the calibration sequence used for tracking. The calibration sequence measures the light that is reflected when there is no retroreflector present.

5.3 Timeline

Table 3. BELLE Technical Task Schedule.

Tasks	Completion (%)	Feb.	Apr.	Jun.	Aug.	Oct.	Nov.
Purchase of laser and performance testing	100	→		→			
Purchase of solar panel and performance testing	100		→	→			
Optical evaluation of laser beam propagation	100			→			
Development of a laser tracking system	100		→	→	→	→	→
Purchase of rover and testing	100			→			
Demonstration of laser-powered rover travel	100					→	
Optimization of the system	100						→
Completion of the prototype system and testing	100						→

5.5 Budget

Table 4. BELLE Budget Summary

	Phase 1	Phase 2
Phase Budget	**$56,684.18**	**$66,912.28**
Wages	$10,572.13	$17,504.21
Materials & Supplies	$9,982.87	$0
Equipment	$10,631.45	$0
UVA Overhead	$21,585.62	$25,480.51
Other Services	$96.81	$0
Rental of Off-Site Facilities	$323.55	$0
Phase Totals	$53,192.43	$42,984.72
Remaining funds	$3,491.75	$23,927.56
Project Total		**$96,177.15**
Remaining funds		**$27,419.31**

5.6 Safety Plan & Protocols

The main hazard is the 100 W fiber-coupled direct diode laser; high-powered lasers can cause irreversible damage to skin and eyes. Team members have been briefed on safety protocols in accordance with UVA's laser safety program. Every team member has been provided with the required laser personal protective equipment. The laser was mounted at or below waist height with the beam path cleared before turning on the laser. A beam dump was used at the end of the path to capture stray laser light. The lab has proper safety precautions for Class IV lasers, such as appropriate laser warning signs, "laser on" warning light, laser stop switch, and sealed and covered windows and doors.

5. Path to Flight

6.1 Overview

The following sections outline future work that needs to be addressed for BELLE to have a successful path to flight. These issues include changes in circuit design, optics, radiation, and thermal control. It is understood that further implementation of BELLE will require further testing and additional research.

6.2 Hardware Design

An improvement that could be made with the benefit of a longer development cycle would be to integrate all the sensor and scanning circuitry on a single printed circuit board. Using a prototype circuit on a perforated board along with separate development MCU's connected by breadboard wires no doubt introduced noise into the system that could be eliminated by moving to a PCB. This would also allow faster transmission speeds between the two MCU's, increasing system performance.

A further improvement would be to replace the built-in analog-to-digital converters in the MCU's that were used to read the sensor values with a higher precision external ADC. In combination with the use of additional filtering discussed later in the optics section, a higher-precision ADC measurement could allow the system to detect much weaker signals reflected from the rover, which could significantly increase the range of the tracking system.

The LED breadboard circuit can be moved to a perforated board for more permanent usage. This would allow more stability of the circuit and decrease the chance of wires getting caught in the rover. Also, the LCD display could be permanently attached to the rover and constantly display the battery percentage along with the current draw into the battery.

Finally, using radiation-hardened components and redundant computation methods could make the system much more resistant to the radiation it would experience on the moon. By using multiple microcontrollers that checked each other's computation in combination with radiation shielding for the embedded system, the probability of system degradation in the extraterrestrial environment could be greatly reduced.

6.3 Optics

One major area for improvement in our design would be the use of a customized optical isolator. Currently, the reflected laser light travels back to the laser, and the slightly expanded beam illuminates the photodiodes. This is not an ideal setup because the photodiodes need to be spread around the collimator and would perform better in a tighter alignment. Additionally, reflecting light back into the laser could damage the optical fiber. One potential solution to this problem would be to use an optical isolator. An optical isolator uses a faraday rotor and two polarizing filters to prevent any light from passing through the first polarizing filter on the return journey. A modification to this setup that would better suit the project would be to set the first polarizing filter at a 45-degree angle so that on the return journey, the light would reflect the side, where it would be ideal for placing the photodetectors.

An additional simple change would be to place infrared bandpass filters over the photodiodes, which would eliminate undesired noise in the signal reading. One significant challenge faced by the team was calibrating the sensors to function well in a wide range of ambient light conditions, an issue that would also be somewhat present on the moon. By placing filters over the photodiodes, the sensitivity could be greatly increased while still retaining a usable signal-to-noise ratio.

6.4 Software

Several improvements could be made to the software to increase the performance and enable more precise and rapid tracking. One primary improvement that could be considered would be to move from the MbedOS C++ library to a bare-metal approach written in C to optimize for additional speed. Although the configuration features of Mbed and the object orientation of C++ assisted for easier software development, a second iteration of the software library written in C could perform more rapidly.

Furthermore, the method of calibrating the sensors could be refined to use a more advanced statistical method. A simple averaging method was used to determine the threshold of illumination required to be considered a reflection from an actual sensor. More advanced statistical methods of calculating sensor threshold could increase the sensitivity of the system and allow it to track at a greater distance.

6.5 Photovoltaic Cell Performance Optimization

A more robust thermal management system of the photovoltaic array could greatly increase the charging rate and power delivery capability of the system. Currently, the array is limited primarily by thermal losses. As the array heats up under the intense radiation of the beam, it rapidly drops in efficiency. This also likely reduces the lifetime of the array. In a lunar environment, the extremely cold ambient temperature could be utilized along with radiators or some other method of heatsinking to significantly increase the heat dissipation of the array. This would allow it to accept much greater laser power intensities without overheating.

6.6 Radiation Control

The radiation on the surface of the moon is roughly 1300 microsieverts a day, approximately 2.6 higher than that seen on the ISS and nearly 200 times higher than what we experience on Earth. This poses a risk of degrading optical components and circuitry and adversely affecting system performance. The source of this radiation is from three key types of ionizing radiation. The first two, the solar wind and solar flares, are produced by the Sun. The third type has its origin outside the solar system and is known as galactic cosmic rays [10]. Figure 22 depicts different types of radiation and the potential adverse effects they could cause:

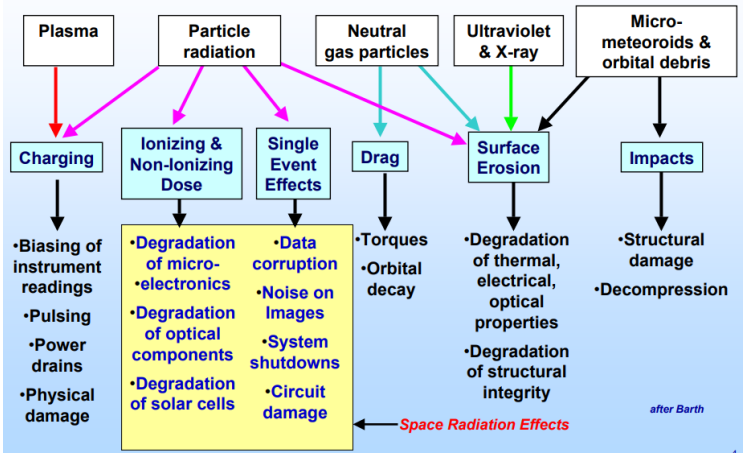

Figure 22. Potential adverse effects of different types of radiation.

As seen in the yellow box in the Figure 22, the main concerns of ionizing radiation are in the degradation of optical components and in-circuit damage. In optical components, which are used extensively in the BELLE system design, changes in the ellipticity of the beam and radiation-

induced lattice damage can occur [11]. The following strategies could be employed to mitigate these risks.

A shielding material could be used to prevent major ionizing radiation. Graded-Z shielding, which consists of a laminate of several materials with different atomic numbers, could be effective. In a typical graded-*Z* shield, the high-*Z* layer scatters protons and electrons and absorbs gamma rays. In extraterrestrial environments, hydrogen-rich elements are effective, and so a shield consisting of polyethylene and Kevlar could be implemented. The material is lightweight compared to single-material shielding, and only about 10g/cm^2 of material is required to reduce the radiation dose by 55% [12].

Figure 23 shows the various forms of ionizing radiation and the material used for preventative measures. To protect circuit elements and data, the proposed solution is to prevent errors within the system by using redundant elements and error-correcting memory. To check for circuit damage and prevent further corruption, redundant elements can be used to check if data is being processed correctly.

Furthermore, additive logic error checkers could be implemented. Such a logic error checker uses extra parity bits to see if data is being processed correctly. This could significantly reduce the probability of data corruption. By using both radiation shielding and redundant hardware mechanisms, the system can hopefully avoid radiation caused degradation.

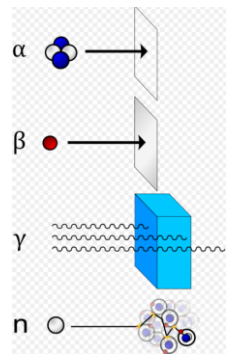

Figure 23. Transmission depths of various subatomic particles.

6.7 Thermal Control

The key challenge in thermal management will be the wide temperature variations experienced on the moon. Lunar temperatures can vary from 127℃ during the day to -183 ℃ during the night. In 2019, China's Chang'e-4 was launched and will have the ability to collect temperature data on the dark side of the moon. This recent discovery can work hand in hand with our proposed BELLE project. With such temperature extremes, thermal management to protect circuitry and other optical components in the system are essential [13].
To protect BELLE subsystems from failing in these wide temperature ranges, a thermal insulation coating could be employed. Such a coating, in addition to maintaining a constant system temperature, could also provide protection from solar flares. Thermal insulation is often implemented in the form of a multi-layered insulator blanket. The industry standard for these blankets contain micron-aluminized Mylar, depicted in Figure 24 below.

Figure 24. The internal structure of a micron-aluminize Mylar sheet, a potential thermal insulator for the BELLE system.

Such a blanket could house the different components of the system. Additionally, a small amount of energy from the solar collection system on the rim of the crater could be diverted towards heating or cooling the system. Due to the insulating properties of the mylar blanket, the system would retain heat very effectively, meaning the total energy required to maintain system temperature once in equilibrium could be quite small.

In addition to the wide temperature ranges on the surface of the moon, the comparatively frigid temperatures seen in permanently shadowed regions prevent additional challenges. Traditionally, most space technologies have used solar energy to keep their systems operating effectively. However, due to the intense cold temperatures and lack of sunlight in PSR's, alternative methods of heating are required. Radioisotope heater units are often used as an efficient alternative heat source and could be implemented in our rover design. These heating units are incredibly small and offer efficient heating for each of the different components. By using radioisotope heater units, additional electric power can be allocated to the performance of circuit components and other electronics. An RHU contains a Pu-238 fuel pellet about the size of a pencil eraser and outputs about 1 Watt of heat [14].

Finally, thermal management will be required for the laser system. An effective approach could involve a copper heatsink coupled to the surface of the laser system with a thermal compound. This heat sink could actively be cooled using several methods, including a thermoelectric device or water-cooling system. It could also be dissipated through a radiator or via the use of heat pipes. The lunar environment presents numerous thermal challenges, but through sound heat management, we believe these challenges can be handled effectively and efficiently.

6. Conclusion

A reliable power delivery system is essential for sustained exploration in the Moon's PSRs; BELLE offers a truly ingenious and low-cost solution using wireless power transmission coupled with a novel tracking algorithm. BELLE eliminates the need for assets to live on single battery life or to leave the PSRs to be recharged, reducing mission costs and risks. Despite COVID, BELLE demonstrated a robust power-beaming proof-of-concept; A fiber-coupled direct diode laser, steered by a dual-axis galvanometer, coupled with multi-junction III-V semiconductor-based solar cells successfully tracked a high-speed rover and powered a load wirelessly.

7. References

[1] K. Watson, B. Murray, and H. Brown, "On the possible presence of ice on the Moon," J. Geophys. Res., vol. 66, no. 5, pp. 1598–1600, May 1961, doi: 10.1029/JZ066i005p01598.

[2] G. Bennett et al., "Mission of Daring: The General-Purpose Heat Source Radioisotope Thermoelectric Generator," presented at the 4th International Energy Conversion Engineering Conference and Exhibit (IECEC), San Diego, California, Jun. 2006, doi: 10.2514/6.2006-4096.

[3] P. Jaffe and J. McSpadden, "Energy Conversion and Transmission Modules for Space Solar Power," Proc. IEEE, vol. 101, no. 6, pp. 1424–1437, Jun. 2013, doi: 10.1109/JPROC.2013.2252591.

[4] M. Kanskar, T. Earles, T. Goodnough, E. Stiers, D. Botez, and L. J. Mawst, "High-power conversion efficiency Al-free diode lasers for pumping high-power solid-state laser systems," San Jose, California, United States, Apr. 2005, p. 47, doi: 10.1117/12.597097.

[5] Andrew McIntosh, "PowerLight Technologies is developing wireless 'power beaming,'" Jan. 29, 2018. https://powerlighttech.com/2018/01/29/powerlight-technologies-is-developing-wireless-power-beaming/

[6] G. Faraci, A. Raciti, S. A. Rizzo, and G. Schembra, "Green wireless power transfer system for a drone fleet managed by reinforcement learning in smart industry," Applied Energy, vol. 259, p. 114204, Feb. 2020, doi: 10.1016/j.apenergy.2019.114204.

[7] J. Haruyama et al., "Lack of Exposed Ice Inside Lunar South Pole Shackleton Crater," Science, vol. 322, no. 5903, pp. 938–939, Nov. 2008, doi: 10.1126/science.1164020.

[8] M. Kanskar, T. Earles, T. J. Goodnough, E. Stiers, D. Botez, and L. J. Mawst, "73% CW power conversion efficiency at 50 W from 970 nm diode laser bars," Electron. Lett., vol. 41, no. 5, p. 245, 2005, doi: 10.1049/el:20058260.

[9] R. R. King et al., "Advances in High-Efficiency III-V Multijunction Solar Cells," Advances in OptoElectronics, vol. 2007, pp. 1–8, 2007, doi: 10.1155/2007/29523.

[10] Lewis, R. H. (n.d.). *Human Safety in the Lunar Environment* (Tech.). Retrieved from https://space.nss.org/settlement/nasa/spaceresvol4/human.html#:~:text=The%20Moon's%20surface%20is%20exposed,known%20as%20galactic%20cosmic%20rays.

[11] Phifer, C. C. (2004). *Effects of Radiation on Laser Diodes* (pp. 1-30, Tech.). Albuquerque, New Mexico: Sandia National Laboratories.

[12] Narici, L., Casolino, M., Di Fino, L. *et al.* Performances of Kevlar and Polyethylene as radiation shielding on-board the International Space Station in high latitude radiation environment. *Sci Rep* 7, 1644 (2017). https://doi.org/10.1038/s41598-017-01707-2

[13] Whitney, J. (2019, January 15). China's Chang'e-4 to take the far side of the moon's temperature for the first time. Retrieved from https://www.intelligent-aerospace.com/home/article/16543412/chinas-change4-to-take-the-far-side-of-the-moons-temperature-for-the-first-time.

[14] Light-Weight Radioisotope Heater Unit. (2017, November 02). Retrieved from https://rps.nasa.gov/power-and-thermal-systems/thermal-systems/light-weight-radioisotope-heater-unit/

[15] "RC LiPo Battery Guide: Explanation, Saftey and Care." http://learningrc.com/lipo-battery/.